REGULAR PAPERS

Experimental study on the pressure wave propagation in the artificial arterial tree in brain

View the article online for updates and enhancements.

REGULAR PAPER

Experimental study on the pressure wave propagation in the artificial arterial tree in brain

Shinya Shimada[1], Ryo Tsurusaki[1], Fumiaki Iwase[1], Mami Matsukawa[1*], and Pierre-Yves Lagrée[2]

[1]*Laboratory of Ultrasonic Electronics, Doshisha University, Kyotanabe, Kyoto 610-0321, Japan*
[2]*CNRS, UMR 7190, Institut Jean Le Rond d'Alembert, Sorbonne University, F-75005 Paris, France*

*E-mail: mmatsuka@mail.doshisha.ac.jp

A pulse wave measurement is effective for the early detection of arteriosclerosis. The pulse wave consists of incident and reflected waves. The reflected wave of the pulse wave measured at the left common carotid artery seems to originate from the vascular beds in the brain. The aim of this study is to know if the reflected waves from the occlusions in cerebral arteries can affect the pulse waveform. The artificial arterial tree in the brain was therefore fabricated using polyurethane tubes. After investigating the effects of the bifurcation angle on the pulse waveform, we attempted to confirm whether the reflected waves from occlusions in the artificial arterial tree in the brain can be experimentally measured at the left common carotid artery. Results indicate that the bifurcation angle did not affect the pulse waveform, and that the reflected wave from an occlusion with a diameter of more than 1 mm in the brain could be observed. © 2018 The Japan Society of Applied Physics

1. Introduction

Cardiovascular diseases (CVDs), including heart disease and stroke, are considered to be one of the leading causes of death in the world. The initial symptom of CVDs is arteriosclerosis, which can be suddenly fatal before medical treatments. Therefore, the early detection of arteriosclerosis is neccessary.[1–7] In the early stage of arteriosclerosis, the arterial stiffness increases extremely, compared with the normal arterial stiffness. Cholesterol plaques are then deposited on the inside walls of arteries, which will be a critical stenosis blocking the blood flow in arteries. For evaluating the arterial stiffness in vivo, the pulse wave, which is the displacement of the skin surface caused by the intravascular pressure arising from the constriction of the heart, is considered to be effective.[6–12]

The pulse wave velocity (PWV) technique, which can measure the propagation velocity in blood vessels, is now used as a diagnostic method.[9–14] According to the Moens–Korteweg equation, the pulse wave velocity appears to be proportional to the square root of the average Young's modulus of arterial walls.[15] It has also been reported that the PWVs of elderly patients were higher than those of young patients.[16] However, the accuracy of the PWV technique is not sufficient for evaluating the arterial stiffness. In addition, this technique only focuses on the propagation velocity of the pulse wave in blood vessels and does not utilize the other fruitful information contained in the pulse wave.[17,18] By developing an advanced technique that can analyze the pulse waveform in more detail, we will evaluate the arterial stiffness more accurately.

The measured pulse wave consists of incident and reflected waves. The incident wave is caused by the blood flow ejected from the heart. After propagating over a long distance between the heart and the ends of peripheral vessels, the incident wave is reflected at the vascular beds. This is called the reflected wave.[2,18–22] Since the attenuation of the reflected wave is strongly dependent on the characteristics of arterial walls, analyzing the reflected wave extracted from the entire pulse wave is more effective for the evaluation of arterial stiffness.

In previous studies, in order to detect pulmonary hypertension, Hanya et al. and Khir and Parker, have focused on the magnitude of the reflected wave obtained by the analysis of the pressure-velocity loop (PV-loop).[21,22] Kanai and coworkers, have also attempted to observe the pulse waveform from the displacement of the carotid arterial wall as a function of time using an ultrasonic diagnostic system.[23–26] As a simple screening method for evaluating the arterial walls, we proposed a new technique of estimating the reflected wave by measuring both the pulse wave and blood flow velocity simultaneously.[6,7] The pulse wave of young and elderly patients was actually measured at the left common carotid artery using a piezoelectric transducer. As a result, the characteristics of arterial walls seemed to affect the pulse waveform. Therefore, we have attempted to elucidate the complex propagation phenomena of these waves by experiments using viscoelastic tubes. The results of previous experiments verified that the pulse waveform changed owing to arterial stiffness and most of the reflected waves measured at the common carotid artery originated from the vascular beds in the brain.[27–29] However, it was difficult to observe the effects of stenosis in cerebral arteries on the pulse waveform owing to the other reflected waves from vascular beds. We still have to investigate whether a critical stenosis in cerebral arteries can change the pulse waveform.

The aim of this study is to know if the reflected wave from a small occlusion in cerebral arteries can affect the pulse waveform. To observe the reflected wave from an occlusion in each cerebral artery, the artificial arterial tree in the brain was fabricated using polyurethane tubes. First, the effects of the bifurcation angle on the pressure waveform were investigated. After confirming that the bifurcation angle does not change the pressure waveform, we attempted to observe the reflected wave from each model occlusion in the artificial arterial tree. This model was composed of eight types of artificial arteries. The diameter and thickness of the tubes were determined from the actual configuration of each cerebral artery.[30–32] For the validation of the measured data, we also discuss the measured data with the theoretical estimation obtained from the one-dimensional (1D) theoretical model.[33,34]

2. Experimental methods

2.1 Fabrication of bifurcation tube and arterial tree

The viscoelastic tubes mimicking blood vessels were fabricated using polyurethane gel (Exseal Asker-C 5). Young's moduli of the tubes were measured using a tensile test apparatus (Shimadzu Ez-Test). Rectangular tensile specimens were fabricated from the tubes, because it was very difficult to fabricate dumb-bell specimens accurately. The actual length, width, and thickness of the tensile specimens were 40, 10, and 2 mm, respectively.

In accordance with the results of the tensile test, the Young's modulus of the tubes was 180 kPa, which would be a slightly higher than those of actual arteries.[35,36] However, the difference between these Young's moduli seems negligible because of the non uniform elastic properties of actual arteries.

When a bifurcation tube is fabricated, the reflection coefficient R_c should be as low as possible. If the radius changes caused by the pressure were small, the reflection coefficient for a perfect bifurcation is approximately defined as[27–29]

$$R_c = \frac{Y_1 - \sum_2^N Y_n}{Y_1 + \sum_2^N Y_n}, \qquad (1)$$

$$Y = \frac{A}{\rho c}, \qquad (2)$$

where Y_1 and Y_n are the admittances of the mother and daughter tubes, respectively. N is the number of daughter tubes connected to the mother tube. A is the cross-sectional area and ρ is the density of liquid. c is the propagation velocity of the pressure wave, which is expressed as

$$c = \sqrt{\frac{Eh}{\rho D}}, \qquad (3)$$

where E, h, and D are the Young's modulus, thickness, and diameter of the tubes, respectively. The actual pressure wave propagation velocities in the artificial arteries might be slightly higher than those calculated using Eq. (3), as shown in Sect. 3.1. This might be because Eq. (3), Moens–Korteweg equation, does not take into account the effects of the viscosity of the tube walls. However, the differences between actual and theoretical pressure wave propagation velocities would be small, in the range of 10 to 15%. For this reason, the Moens–Korteweg equation can be used to estimate the theoretical pressure wave propagation velocities in the viscoelastic tubes.

In the case of actual arterial bifurcations in the brain, the wave reflection at a bifurcation point does not occur.[2,27,33] As for the bifurcation tubes, the reflection coefficient R_c depends on the Young's modulus, diameter, and thickness of the mother and daughter tubes, as shown in Eq. (3). In light of the difficulty in changing the Young's modulus, the diameter and thickness of the daughter tubes should be determined from the configurations of the mother tube and actual arteries to maintain the reflection coefficient as low as possible. Otherwise, the reflection at a bifurcation tube might occur owing to the inappropriate reflection coefficient.

Table I. Details of the bifurcation tube (unit in mm).

No.	Name	Inner diameter	Thickness
①	Left common carotid artery	8.0	2.0
②	External carotid artery	6.0	2.0
③	Internal carotid artery	6.0	2.0
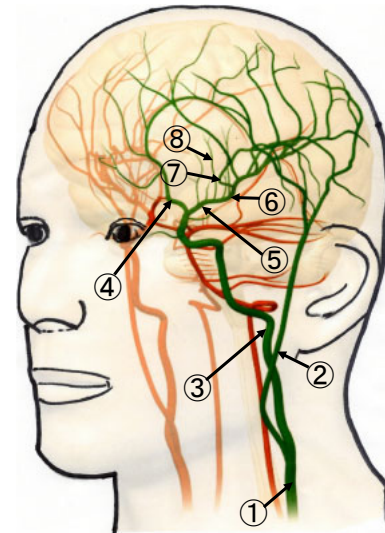
Fig. 1. (Color online) Image of cerebral arteries.

Table II. Details of the artificial arterial tree in brain and estimated reflection coefficient of each reflected wave (unit in mm).

No.	Name	Inner diameter	Thickness	Reflection coefficient (%)
①	Left common carotid artery	8.0	2.0	N/A
②	External carotid artery	6.0	2.0	N/A
③	Internal carotid artery	6.0	2.0	38
④	Anterior cerebral artery	4.0	1.0	24
⑤	Proximal middle cerebral artery	4.0	1.0	24
⑥	Distal middle cerebral artery	3.0	1.0	15
⑦	Prefrontal artery	2.0	1.0	4
⑧	Lenticulostriate artery	1.0	1.0	0.54

To investigate the effects of the bifurcation angle on the pressure waveform, three bifurcation tubes with bifurcation angles of 45, 90, and 180° were fabricated. The diameter and thickness of each tube were determined from the configuration of each artery and are shown in Table I. It was also reported that the angle of the common carotid branch to form the internal and external carotid arteries ranges from 10 to 50°.[37] The arterial branches with an angle of more than 50° would exist in the brain. Next, we fabricated an artificial arterial tree in the brain. This model was composed of 8 types of artificial arteries presented in Fig. 1. The diameter and thickness of each tube can be seen in Table II.[30–32] The thicknesses of the actual lenticulostriate and prefrontal arteries are less than 1 mm.[30,31] However, it was not possible to fabricate the tubes with a thickness of less than 1 mm, and the small difference in thickness does not significantly change
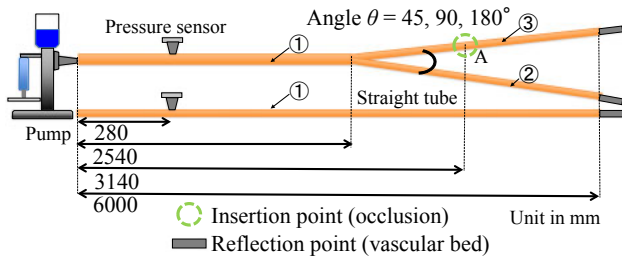
Fig. 2. (Color online) Experimental systems for the investigation of the effects of bifurcation angle on the pressure waveform and the measurement of the reflected wave from the internal carotid artery occlusion.
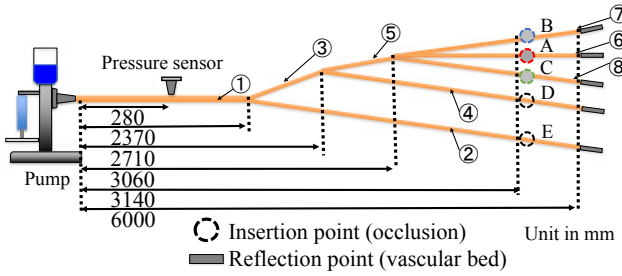
Fig. 3. (Color online) Experimental system for the measurement of the reflected wave from the occlusions in the artificial arterial tree.

the measured data, considering the pressure perturbation law written below.

2.2 Experiments

As shown in Figs. 2 and 3, experimental systems consisted of a pump (TOMITA Engineering, custom-made) mimicking the heart and artificial arteries. The pump ejected a half cycle of a sinusoidal wave to the tubes as an input flow. The ejection time and volume of an input flow were 0.3 s and 4.5 ml, respectively. The estimated wavelength of the initial pressure wave was 4.8 m. The inner pressure in the arterial tree was measured using a pressure sensor (Keyence AP-10S). Determined as the distance between the heart and the left common carotid artery, the measurement point was located 280 mm away from the ejection point.

First, the effects of the bifurcation angle on the pressure waveform were investigated. As shown in Fig. 2, two stainless rods were inserted at the end of the tubes to imitate reflections at vascular beds. The bifurcation point was located 2540 mm away from the ejection point to prevent the overlapping of the expected reflection at the bifurcation point and the incident wave ejected from the pump. To confirm whether a reflected wave from the bifurcation point occurs, the total length of the tubes, namely, from the ejection point to the end of the tubes, was set to 6000 mm, which was much larger than the pressure wavelength of 4.8 m and sufficiently far away from the bifurcation point. This enabled us to only observe the reflected wave from the bifurcation point. After confirming that the bifurcation angle does not affect the pressure waveform, we set a stainless rod as an internal carotid artery occlusion at insertion point A in Fig. 2, which was located 3140 mm away from the ejection point. To measure the reflected wave from the internal carotid artery occlusion separated from the initial pressure waves, the total length of the tubes was set to 6000 mm because this reflected wave was expected to be very large and might overlap with

the other reflected waves. This result was used to validate the pressure wave propagation in the artificial bifurcation tube by comparison with the theoretical estimation.

Next, the reflected wave from each model occlusion in the arterial tree in the brain was measured. The experimental system used is shown in Fig. 3. Five stainless rods were inserted at the end of the tubes to imitate reflections at vascular beds. Next, a stainless rod was set as a cerebrovascular occlusion at insertion point A, B, or C, which was located 3140 mm away from the ejection point. To observe a reflected wave separated from pressure waves, the total length of the tubes was set to 6000 mm as described previous.

2.3 1D theoretical model

For the validation of the measured data obtained from the experiments, the 1D theoretical model composed of the following governing equations was applied.[33,34]

Conservation of mass:

$$\frac{\partial A}{\partial t} + \frac{\partial Q}{\partial x} = 0. \tag{4}$$

Momentum equation:

$$\frac{\partial Q}{\partial t} + \alpha \frac{\partial}{\partial x}\left(\frac{Q^2}{A}\right) = -\frac{A}{\rho}\frac{\partial P}{\partial x} - \frac{C_f Q}{R^2}. \tag{5}$$

Here, Q is the average flux over the cross section of each tube, A and α are the velocity profile factor. ρ and C_f are the fluid density and friction term, respectively. P is the inner pressure in the viscoelastic tubes.

The pressure perturbation law is expressed as

$$P = \frac{Eh}{(1-\sigma^2)R_0^2}[(R-R_0) + \varepsilon_p(R-R_0)^2] + \eta\frac{\partial R}{\partial t}, \tag{6}$$

where E is Young's modulus, h is the thickness, σ is Poisson's ratio, ε_p is the coefficient of the nonlinear stress strain characteristics, η is the viscosity of the arterial wall, R is the radius of tube. R_0 is the unperturbed radius. We used the thickness and radius in Table I for the 1D theoretical model.

By changing the unknown parameters E, η, ε_p, α, and C_f, the optimum parameters used to describe the measured data were determined. In this study, the 1D theoretical model was used to validate the observed reflected wave from the internal carotid artery occlusion. Only when the 1D theoretical model was applied to the validation of pressure wave propagation in the bifurcation tube, the boundary conditions at a bifurcation point in the experiments were used for simulating the dynamics in a bifurcation tube.[33] Since the pressure wave was not attenuated at a bifurcation point in the experiments, we assumed that the pressure wave propagation at a bifurcation point was ideal.[27,33]

3. Results and discussion

3.1 Effects of the bifurcation angle

Figure 4(a) shows the effects of the bifurcation angle on the pressure waveform as a function of time. The first peak observed at approximately 0.3 s is an incident wave ejected by the pump. The second peak reflected at the end of the tubes, placed 6000 mm away from the ejection point, can be seen at approximately 1.6 s. If the reflected wave from the bifurcation point had occurred, it could have been measured between the first and second peaks. However, the reflected
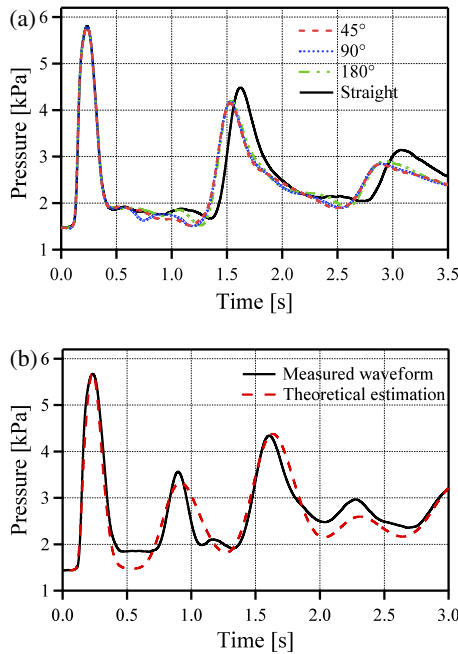
Fig. 4. (Color online) (a) Effects of the bifurcation angle on the pressure waveform. (b) Comparison of the measured and theoretical waveforms. Observed reflected wave from the internal carotid artery occlusion in the simple bifurcation tube.

Table III. Estimated optimum value of each parameter.

Young's modulus E (kPa)	185
Viscosity of tube wall η	0.085
Nonlinear term ε_p	0.041
Velocity profile factor α	1.0
Friction term C_f	2.5

Fig. 5. (Color online) (a) Observed reference wave in the artificial arterial tree in brain. (b) Observed reflected wave from each occlusion in the artificial arterial tree in brain.

wave from the bifurcation point was not observed, even when the bifurcation angle was changed in the range of 45 to 180°. This certified that the bifurcation angle did not affect the pressure waveform at all. The pressure wave in the straight tubes without a bifurcation propagated more slowly, as you can see in the second and third peaks observed at approximately 1.6 and 3.0 s, respectively. This is because the actual pressure wave propagation velocities in the artificial common and internal carotid arteries were approximately 7.5 and 9.0 m/s, respectively. These velocities can be obtained using the propagation distances and arrival times of the first peaks of the pressure waveforms, measured 280, 560, 840, and 1120 mm away from the ejection point in the straight tubes.

According to Eq. (3), the pressure wave propagation velocity depends on the Young's modulus, diameter, and thickness of the tubes. The pressure wave propagation velocities in the artificial common and internal carotid arteries calculated using Eq. (3) were 6.7 and 7.7 m/s, respectively. Since the differences between the actual and theoretical pressure wave propagation velocities were in the range of 10 to 15%, the actual pressure wave propagation velocities in these artificial arteries were in good agreement with the estimated velocities. From the above discussions, the arrival time difference of the second peaks observed at around 1.6 s should be approximately 0.1 s in Fig. 4(a). Therefore, the pressure wave propagation velocity in the straight tubes was lower since the diameter of the straight tubes without a bifurcation was 2 mm larger than that of the mother tubes of the bifurcation tubes.

3.2 Comparison of the measured data and theoretical estimation

After confirming that the bifurcation angle does not change the pressure waveform, we observed the reflected wave from a stainless rod used as the internal carotid artery occlusion in
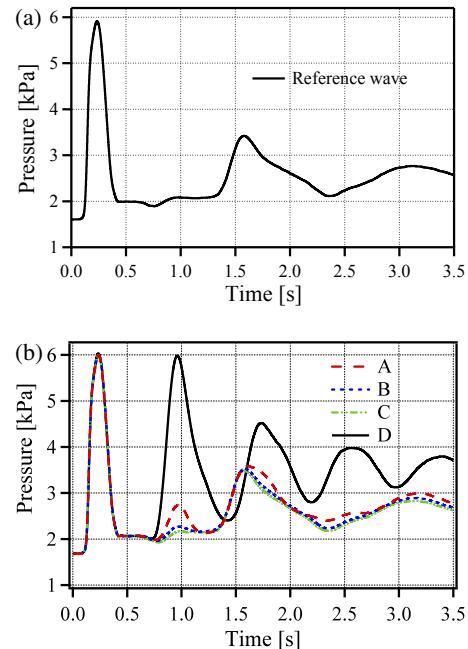
the bifurcation tube. The 1D theoretical model was also applied to validate the measured reflected wave from the internal carotid artery occlusion.[33,34] The comparison of the measured and theoretical waveforms can be seen in Fig. 4(b). The optimum parameters used to evaluate the measured data were also determined, as shown in Table III. As a result, the large reflected wave from the internal carotid artery occlusion, placed 3140 mm away from the ejection point, was observed at around 0.8 s. The incident wave ejected by the pump was observed at around 0.3 s. The reflected wave from the end of the tube located 6000 mm away from the ejection point was measured at around 1.6 s. The theoretical estimation was also in good agreement with the measured waveform. This indicates that the experiments using the bifurcation tubes are valid for the clarification of pressure wave propagation phenomena in an actual arterial bifurcation.[27–29]

3.3 Observation of the reflected waves from occlusions

First, after the stainless rods were inserted at all the reflection points in Fig. 3, the pressure wave was measured as a reference wave without placing any stainless rods at the insertion points. The reference waveform can be seen in Fig. 5(a). The incident wave ejected by the pump was observed at around 0.3 s as the first peak. The second peak observed at around 1.6 s was the reflected waves from the end of the tubes located 6000 mm away from the ejection

point. If a stainless rod is inserted at insertion point A, B, or C as an occlusion, the reflected wave from the model occlusion can be measured between the first and second peaks. The static pressure in the tubes also increased owing to the input flow ejected by the pump.

Figure 5(b) shows four observed pressure waveforms as a function of time. The stainless rod was inserted at insertion point A. Result [A] represents the waveforms reflected from insertion point A and the other reflection points. The reflected wave from insertion point A can be seen at around 0.9 s. The amplitude of this reflected wave, P_A, subtracted from the static pressure, was 0.56 kPa.

Secondly, the stainless rod at insertion point A was removed and inserted at insertion point B. Result [B] shows the reflected wave from insertion point B and the other reflection points. The reflected wave from insertion point B was also measured at around 0.9 s. The amplitude of this reflected wave, P_B, was 0.14 kPa.

Next, the stainless rod at insertion point B was removed and inserted at insertion point C. Result [C] shows the reflected wave from insertion point C and the other reflection points. The reflected wave from insertion point C can be seen at around 0.9 s, too. The amplitude of this reflected wave, P_C, was 0.02 kPa.

Finally, the additional stainless rods were inserted at insertion points A, B, D, and E. Result [D] represents the total reflection of incident waves from insertion points A, B, C, D, and E. The total reflection from all the insertion points was observed at around 0.9 s. The amplitude of this total reflection, P_D, was 3.68 kPa.

As you can see in the reflected waves from the model occlusions, the arrival times of the reflected waves were almost the same. The distance between the bifurcation point and each model occlusion was 80 mm, and the pressure wave propagation velocities in the artificial middle cerebral, prefrontal, and lenticulostriate arteries were theoretically 7.7, 9.4, and 13.4 m/s, respectively, in accordance with Eq. (3). Therefore, the arrival time difference of the reflected waves from the model occlusions should be in the range of 0.04 to 0.08 s. This indicates that it is too difficult to recognize the arrival time differences of the reflected waves on the scale of the horizontal axis in Fig. 5(b).

By dividing P_A, P_B, and P_C by P_D, the reflection coefficients were estimated, as shown in Table II. The attenuation of each tube is expected to vary, depending on the diameter and thickness of the tubes. Although the propagation distance of the reflected wave was much larger than the actual length of cerebral arteries, the reflected wave from the stainless rod with a diameter of 1 mm was visible. Therefore, there is a possibility that the reflected wave from an occlusion with a diameter of more than 1 mm in the brain may be observable at the left common carotid artery in vivo.

4. Conclusions

In this study, the artificial arterial tree in the brain was fabricated to elucidate the complicated pressure wave propagation phenomena in arteries. This model was composed of eight types of artificial arteries presented in Fig. 1 and Table II. The inner diameters of the artificial middle cerebral, prefrontal, and lenticulostriate arteries were 3, 2, and 1 mm, respectively. The thicknesses of these arteries

were set to 1 mm. Next, we investigated the effects of the bifurcation angle on the pressure waveform and attempted to observe the reflected pulse wave from the model occlusion with a diameter of more than 1 mm in a brain artery model at the left common carotid artery experimentally. As a result, we confirmed that the bifurcation angle did not affect the pulse waveform at all. Under these conditions, the large reflected wave from the stainless rod used as the internal carotid artery occlusion was observed at the left common carotid artery. This measured data showed good agreement with the waveform obtained from the 1D theoretical model.

We could also measure the reflected waves from the model occlusions of the middle cerebral, prefrontal, and lenticulostriate arteries in the experiments. Therefore, an occlusion with a diameter of more than 1 mm in cerebral arteries possibly changes the pulse waveform in vivo. Here, the reflected wave from the model occlusion of the lenticulostriate artery with a diameter of 1 mm was very small, and the reflection coefficient of this reflected wave was estimated to be 0.54%, as shown in Table II. In light of the attenuation caused by actual arterial walls, it seems difficult to observe the reflected wave from the actual occlusion of the lenticulostriate artery at the common carotid artery in vivo. Therefore, it would be necessary to determine whether the reflected waves from the cerebral occlusions can be measured at the common carotid artery by further clinical research.

1) WHO, Global Status Report on Noncommunicable Diseases (2014).
2) W. W. Nichols and M. F. O'Rourke, *McDonald's Blood Flow in Arteries* (Hodder Arnold, London, 2005) Chaps. 2, 3, 10, and 19.
3) K. Ikeshita, H. Hasegawa, and H. Kanai, Jpn. J. Appl. Phys. **47**, 4165 (2008).
4) K. Ikeshita, H. Hasegawa, and H. Kanai, Jpn. J. Appl. Phys. **48**, 07GJ10 (2009).
5) G. F. Mitchell, H. Parise, E. J. Benjamin, M. G. Larson, M. J. Keyes, J. A. Vita, R. S. Vasan, and D. Levy, Hypertension **43**, 1239 (2004).
6) M. Saito, Y. Yamamoto, M. Matsukawa, Y. Watanabe, M. Furuya, and T. Asada, Jpn. J. Appl. Phys. **48**, 07GJ09 (2009).
7) M. Saito, Y. Yamamoto, M. Matsukawa, Y. Watanabe, M. Furuya, and T. Asada, Jpn. J. Appl. Phys. **49**, 07HF12 (2010).
8) K. Cruickshank, L. Riste, S. G. Anderson, J. S. Wright, G. Dunn, and R. G. Gosling, Circulation **106**, 2085 (2002).
9) E. D. Lehman, J. R. Parker, K. D. Hopskin, M. G. Taylor, and R. G. Gosling, J. Biomed. Eng. **15**, 221 (1993).
10) H. Kanai, K. Kawabe, M. Takano, R. Murata, N. Chubachi, and Y. Koiwa, Electron. Lett. **30**, 534 (1994).
11) B. E. Westerhof, J. P. van den Wijngaard, J. P. Murgo, and N. Westerhof, Hypertension **52**, 478 (2008).
12) A. P. Avolio, S. G. Chen, R. P. Wang, C. L. Zhang, M. F. Li, and M. F. O'Rourke, Circulation **68**, 50 (1983).
13) H. Hasegawa, M. Sato, and T. Irie, Jpn. J. Appl. Phys. **55**, 07KF01 (2016).
14) M. Sato, H. Hasegawa, and H. Kanai, Jpn. J. Appl. Phys. **53**, 07KF03 (2014).
15) M. Stevanov, J. Baruthio, and B. Eclancher, J. Appl. Physiol. **88**, 1291 (2000).
16) A. Qasem and A. Avolio, Hypertension **51**, 188 (2008).
17) T. Kubozono, M. Miyata, K. Ueyama, A. Nagaki, Y. Otsuji, K. Kusano, O. Kubozono, and C. Tei, Circ. J. **71**, 89 (2007).
18) K. Shirai, J. Utino, K. Otsuka, and M. Takata, J. Atheroscler. Thromb. **13**, 101 (2006).
19) J. P. Murgo, N. Westerhof, J. P. Giolma, and S. A. Altobelli, Circulation **62**, 105 (1980).
20) J. P. Murgo, N. Westerhof, J. P. Giolma, and S. A. Altobelli, Circulation **63**,

122 (1981).

21) S. Hanya, K. Yoshii, and M. Sugawara, Ann. Vasc. Dis. **10**, 197 (2017).

22) A. W. Khir and K. H. Parker, J. Biomech. **35**, 775 (2002).

23) Y. Miyachi, H. Hasegawa, and H. Kanai, Jpn. J. Appl. Phys. **54**, 07HF18 (2015).

24) Y. Nagai, H. Hasegawa, and H. Kanai, Jpn. J. Appl. Phys. **53**, 07KF19 (2014).

25) K. Nakahara, H. Hasegawa, and H. Kanai, Jpn. J. Appl. Phys. **53**, 07KF09 (2014).

26) Y. Sakai, H. Taki, and H. Kanai, Jpn. J. Appl. Phys. **55**, 07KF11 (2016).

27) Y. Yamamoto, M. Saito, Y. Ikenaga, M. Matsukawa, Y. Watanabe, M. Furuya, and T. Asada, Jpn. J. Appl. Phys. **50**, 07HF12 (2011).

28) Y. Ikenaga, S. Nishi, Y. Komagata, M. Saito, P.-Y. Lagrée, T. Asada, and M. Matsukawa, Proc. IEEE Trans. Ultrason. Ferroelectr. Freq. Control **60**, 2381 (2013).

29) M. Saito, Y. Yamamoto, M. Matsukawa, Y. Watanabe, M. Furuya, and T. Asada, Proc. IEEE Ultrasonics Symp., 2009, p. 1934.

30) S. Marinković, H. Gibo, M. Milisavljević, and M. Ćetković, Clin. Anat. **14**, 190 (2001).

31) S. Sundari, M. Sampath, and J. Jaya Rani, Int. J. Sci. Res. **6**, 19 (2017).

32) J. Krejza, M. Arkuszewski, S. E. Kanser, J. Weigele, A. Ustymowicz, R. W. Hurst, B. L. Cucchiara, and S. R. Messe, Stroke **37**, 1103 (2006).

33) M. Saito, Y. Ikenaga, M. Matsukawa, Y. Watanabe, T. Asada, and P.-Y. Lagrée, J. Biomech. Eng. **133**, 121005 (2011).

34) X.-F. Wang, S. Nishi, M. Matsukawa, A. Ghigo, P.-Y. Lagrée, and J.-M. Fullana, J. Biomech. Eng. **49**, 565 (2016).

35) M. Couade, M. Pernot, C. Prada, E. Messas, J. Emmerich, P. Bruneval, A. Criton, M. Fink, and M. Tanter, Ultrasound Med. Biol. **36**, 1662 (2010).

36) T. Khamdaeng, J. Luo, J. Vappou, P. Terdtoon, and E. E. Konofagou, Ultrasonics **52**, 402 (2012).

37) A. V. Kamenskiy, J. N. MacTaggart, I. I. Pipinos, J. Bikhchandani, and Y. A. Dzenis, J. Biomech. Eng. **134**, 064502 (2012).